A Particle-in-Cell Model for Geophysical Fluid Flows
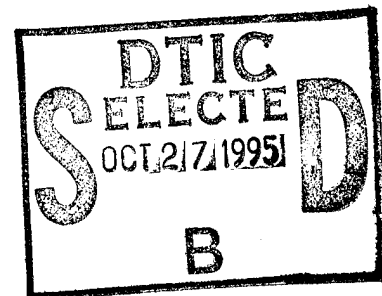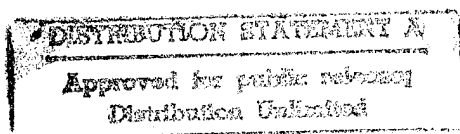
A. D. Kirwan, Jr.

Center for Coastal Physical Oceanography

Old Dominion University, Norfolk, Virginia

C. E. Grosch

Center for Coastal Physical Oceanography and

Department of Computer Science

Old Dominion University, Norfolk, Virginia

J. J. Holdzkom II

Center for Coastal Physical Oceanography

Old Dominion University, Norfolk, Virginia

A.D. Kirwan, Jr.

Center for Coastal Physical Oceanography

Crittenton Hall

Old Dominion University

768 52nd Street

Norfolk, VA 23529

2

Abstract

A particle-in-cell ansatz for solving the Euler equations for geophysical fluid dynamics is described. The approach is ideally suited for "layered" models in which density and velocity are independent of the vertical coordinate in fluid layers but generally vary with layer specification. The material acceleration terms in the Euler equations are solved at each particle while the gradient terms are evaluated on a grid and interpolated at each time step to the particles. Particles are given a specified tetrahedral shape whose base area is equal to four computational cells; however, there are many particles in each cell. The height of each particle is fixed and may be constant for all particles or may vary from particle to particle. In either case criteria are established for the number of particles required for each layer. The efficacy of the model is illustrated by comparing solutions with those from an exact solution of a nonlinear reduced gravity model of a parabolic lens. The particle-in-cell model reproduces the essential characteristics of the reduced gravity model including exceptional resolution of the time varying surface front of the lens.

1 INTRODUCTION

Most simulations of classical fields (electricity and magnetism, elasticity, fluid dynamics) have utilized Eulerian or fixed grid/element techniques. But as noted by Olim [1], time steps utilized by these schemes may be restricted by stability or damping so as to be considerably smaller than the time interval appropriate for the system evolutionary time scale. As a consequence, Lagrangian or particle techniques have become fashionable for problems with large velocities.

With pure Lagrangian techniques, the particles comprise the grid. These methods have long been popular with vortex models since the early work of Christiansen [2] and Christiansen and Zabusky [3]. Some recent examples are Dukowicz and Meltz [4], Winckelmans and Leonard [5] and Russo [6]. However, as pointed out in [1], a potential problem with these methods is the deterioration of spatial resolution in those parts of the calculation domain with low vortex density. Also, with this method it is necessary to calculate a nontrivial interaction of each particle with all other particles at each time step using the Biot-Savart law. Such calculations increase greater than linearly with the number of particles and are particularly susceptible to round-off errors.

Semi-Lagrangian or particle-in-cell (PIC) schemes can overcome some of these problems. With this method all gradient-type terms in the conservation of mass and momentum equations are computed at fixed grid points while the material derivatives are computed at particles. Much of the calculation is devoted to interpolating particle properties to the fixed grid, calculating gradients, and then interpolating gradient values from the grid back to the particles. As with vortex methods there is a trade-off between resolution and number of particles. The computational load for large particle numbers, however, does not appear to be as severe with PIC schemes as it does with vortex models since it increases only linearly with the number of particles. This method was first developed by Harlow [7] for fluids. Since

4

then there have been extensive applications by Brunel et al. [8], Brackbill and Ruppel [9] and O'Rourke et al. [10] to name but a few.

The concern here is with geophysical fluid dynamics. This discipline poses two difficult problems for modelers. One is the enormous range of scales and consequent phenomenology for which the model must account. With basin scale primitive equation Eulerian models the grid spacing generally is much too coarse to resolve all the energetic motions. The other problem is fronts or interfaces. The formation and evolution of many types of atmospheric or oceanographic fronts have no analog in fluid mechanics other than multi-fluid systems. As noted in [10], PIC methods which allow for conservation of a material property at particles can be very effective for tracking material interfaces. Despite their advantages vis-à-vis Eulerian methods there have been very few applications of Lagrangian methods in geophysical fluid dynamics. Notable exceptions are Zabusky and McWilliams [11] and Hooker [12], who used point-vortex models to study geostrophic vortices, and Pavia and Cushman-Roisin [13, 14], Pavia [15] and Mathias [16], who used PIC methods to study ocean fronts and merging of ocean eddies.

The PIC applications in geophysical fluid dynamics have been used in layer models. The model equations result from a vertical integration of the hydrodynamic equations along with an appeal to quasi-hydrostatic equilibrium. If the height of individual particles is specified either a priori or by some pseudo-equation of state then there is no need to calculate the horizontal divergence and solve the conservation of mass equation at each particle. This is considerably simpler than the standard Eulerian approach of solving a Poisson problem for the pressure at each time step. However, there is still the problem of interpolating particle heights to the grid and the gradients back to the particles in a self-consistent manner. A second issue is the number of particles to use. To date, this has been empirically set as an ad hoc balance between accuracy and computational feasibility.

There are several unusual features about our approach. First, we use the full shallow

water hydrodynamic equations. Second, we use an interpolation routine that exactly kills particle self-motion caused by fictitious pressure gradients associated with the distribution of the particle heights on the grid. Moreover, our approach does not require smoothing or damping other than that resulting from the interpolation routines. Finally, we are able to relate the number of particles to a desired spatial resolution. This is achieved by requiring the total volume of particles to be the same as the fluid volume. Since the particle volume is fixed our method guarantees conservation of volume.

2 THEORY

2.1 Two-layer Model

The dynamical basis for the applications considered here are the hydrodynamic equations for a two-layer fluid in a steadily rotating coordinate system. Following the notation of Hurlburt and Thompson [17] these are

$$\frac{d}{dt}\mathbf{v}_1 + \mathbf{k} \times f\mathbf{v}_1 = -g\nabla(h_1 + h_2 + D) + \frac{\tau_S - \tau_I}{\rho_1 h_1} + A\nabla^2\mathbf{v}_1, \tag{1}$$

$$\frac{dh_1}{dt} + h_1\nabla \cdot \mathbf{v}_1 = 0, \tag{2}$$

$$\frac{d}{dt}\mathbf{v}_2 + \mathbf{k} \times f\mathbf{v}_2 = -g\nabla(h_1 + h_2 + D) + g_*\nabla h_1 + \frac{\tau_I - \tau_B}{\rho_2 h_2} + A\nabla^2\mathbf{v}_2, \tag{3}$$

$$\frac{dh_2}{dt} + h_2\nabla \cdot \mathbf{v}_2 = 0, \tag{4}$$

$$\frac{d}{dt} = \frac{\partial}{\partial t} + \mathbf{v}_i \cdot \nabla. \tag{5}$$

In these equations, $\mathbf{v}_i$ is the horizontal velocity vector for layer i; $\mathbf{k}$ is the unit vertical vector; f is Coriolis; g is the gravity constant; h_i are the instantaneous layer thicknesses

relative to a common datum; D is the bottom topography; τ_j are the stresses at the surfaces $j = S$ (upper surface), I (interface between the layers), and B (bottom surface); ρ_i are the constant densities of each layer; A is the horizontal turbulent viscosity; and $g_* = g(\rho_2 - \rho_1)/\rho_2$ is "reduced" gravity. These equations are obtained by vertically integrating the instantaneous three-dimensional hydrodynamic equations. Figure 1 is a cartoon of the geometry for the problem considered below.

As the primary purpose here is to test the efficacy of the PIC method with special cases it will not be necessary to consider either the surface stresses τ_i or turbulent viscosity A. Consequently, these terms will be neglected below. Furthermore, since the test problems studied here are for the "reduced" gravity special case of (1)–(4) it is sufficient to set $D = 0$.

The physical basis for the reduced gravity case is that, to a first approximation, the lower layer only adjusts hydrostatically to accelerations. Hence, there is negligible flow in the lower layer and its thickness gradient ∇h_2 can be eliminated in favor of ∇h_1 from (3) and substituted into (1). The result of this manipulation is

$$\frac{d\mathbf{v}}{dt} + \mathbf{k} \times f\mathbf{v} = -g_*\nabla h, \tag{6}$$

$$\frac{dh}{dt} + h\nabla \cdot \mathbf{v} = 0. \tag{7}$$

As there is flow in only the upper layer, the subscripts denoting layers are superfluous; consequently, they were dropped in (6) and (7) and below.

At this point it is appropriate to nondimensionalize (6) and (7). The scheme used by Cushman-Roisin et al. [18] is appropriate. This scales h by H (representative layer thickness), ∇ by $f/\sqrt{g_*H}$, time by f^{-1}, and $\mathbf{v}$ by $\sqrt{g_*H}$. This scaling removes all explicit parameter dependence. The resulting equations are

$$\frac{d\mathbf{v}}{dt} + \mathbf{k} \times \mathbf{v} + \nabla h = 0, \tag{8}$$

$$\frac{dh}{dt} + h\nabla \cdot \mathbf{v} = 0. \tag{9}$$

Since we use a particle method these last three equations must be augmented by two path equations:

$$\frac{d\mathbf{x}}{dt} - \mathbf{v} = 0. \tag{10}$$

Equations (8)–(10) constitute five nonlinear coupled equations governing the flow in the upper layer. We solve these as an initial value problem using the PIC technique described below.

2.2 PIC Paradigm

The basis of PIC methods is to solve the d/dt terms of (8)–(10) at the particles and the gradient and divergence terms on a discrete grid. Interpolation between the particles and field occurs at each time step. The central assumption of the PIC method as applied to these geophysical fluid dynamics problems is that the heights and volumes of each individual particle are invariant with position and time. Thus there is no need to solve (9) at individual particles. As suggested in [10], keeping each particle height fixed provides a means for accurate tracking of the interface between the active and inert layers.

The height gradient appearing in (8) is found by computing (interpolating) the "h" field to the grid using the positions and heights of the particles, computing ∇h on the grid, and finally computing (interpolating) ∇h back to each particle. In order to clarify these ideas we outline the algorithm. Assume that the position, velocity and height of each particle is known at time t. The steps in the algorithm to advance these data to time $t + \delta t$ are

8

1. interpolate the heights of the particles to the grid,

2. calculate the finite difference approximation to ∇h on the grid,

3. interpolate ∇h from the grid to the particles,

4. using an appropriate time integrator, simultaneously integrate (8) and (10) from t to $t + \delta t$. This yields the position and velocity of each particle at the new time.

For geophysical fluid dynamics problems, the critical issue is the calculation of the height or pressure gradients. In the standard approach used in [13 – 16], the height field is specified as the sum of heights over all particles. Individual particle heights are usually fixed and their base areas are no larger than a computation cell.

An alternate approach is employed here. There are some unique aspects about our method so some explanation is offered. As in prior approaches, each particle is assigned a finite volume where the total volume of the particles is the same as the initial volume of the active layer. We differ from other investigations in that we require the base of each particle to be a square with sides of length 2Δ, where Δ is the fixed distance between cell centers. Thus, a typical particle base has the area of four cells and generally will overlap into nine cells.

The height equation for a particle is

$$z_p = h_p(1 - |\xi_x|/\Delta)(1 - |\xi_y|/\Delta), \tag{11}$$

where (ξ_x, ξ_y) are the component distances of the apex from the nearest cell center. Note that $|\xi_x|, |\xi_y| \le \Delta$. The centerline height of a particle is h_p, which may vary from particle to particle. As can be seen from (11), the height decays linearly to zero at the particle boundaries. This shape was utilized by Hockney and Eastwood [19] who termed it a "triangular-shaped

cloud." Figure 2 is a three-dimensional perspective of this shape. Within any one grid cell there will be considerable overlap of particle bases.

It must be understood that the particles are not to be thought of as solid particles that cannot be interpenetrated but as a computational representation of fluid particles. If several particles were to be located at exactly the same (x, y) location we interpret this as meaning that the height, h, at that location is the sum of the height of the individual particles. These particles do not lose their identity as they interpenetrate and pass through each other and so the number of particles is invariant. There are no particle-particle interactions other than what arise through the gradient of the height field.

The key to our approach is the method by which the height of the particles is apportioned to the centers of cells which they overlie, the method used to calculate height gradients on the fixed grid composed of cell centers, and then the interpolation routine used to move these back to the particles. Our experience has been that these operations are not independent but must be done in an internally consistent fashion. The principle used here is to require that gradients interpolated to a particular particle be independent of the height of that particle. This insures no self-generated motion.

Figure 3 illustrates a typical cross section along the x axis. From (11), the normalized cross-sectional areas of the particle in each of the enveloped cells along this axis are

$$w_{j-1} = (1/2 - \xi_x/\Delta)^2/2,$$

$$w_j = \{1 - (1/2)[1/2 + 2(\xi_x/\Delta)^2]\},$$

$$w_{j+1} = (1/2 + \xi_x/\Delta)^2/2, \tag{12}$$

where the normalization factor is the cross-sectional area of the particle. The interpolation of the height of this particle to the overlapped cell centers is then given by $h_p w_{j-1}$, $h_p w_j$, $h_p w_{j+1}$ for the $j - 1$, j, and $j + 1$ cells, respectively. The hatched, open, and cross-hatched

10

areas in figure 3 show how the height is partitioned at the three grid points.

The above results apply to a typical cross section for a single particle. The two-dimensional case for a generic particle p is achieved by prescribing the weights as

$$w_p(\xi_x^p, \xi_y^p) = w_i(\xi_x^p)w_j(\xi_y^p). \tag{13}$$

To summarize, the height at the ith, jth cell center is the weighted average of all particles enveloping the cell. This is given by

$$h_{i,j} = \sum_{p=1}^{N_{i,j}} w_p h_p, \tag{14}$$

where p is the particle number in the cell and $N_{i,j}$ is the number of particles that overlap into the cell i, j. After the heights are accumulated at all grid points, second order accurate gradients are calculated and then interpolated back to the particles using the same weights. From (14), the values of the gradients at the nine relevant cell centers are readily expressed as

$$D_{i+\alpha,j+\beta} = [h_{i+\alpha+1,j+\beta} - h_{i+\alpha-1,j+\beta}]/2\Delta, \tag{15A}$$

for the x component of the gradient and

$$= [h_{i+\alpha,j+\beta+1} - h_{i+\alpha,j+\beta-1}]/2\Delta, \quad \alpha, \beta = -1, 0, 1, \tag{15B}$$

for the y component.

Interpolation of these gradients back to a particular particle P in cell i, j is independent of h_P. To see this, focus on the x component, (15A). The interpolation of this component back to P is

$$G_{i,j}^P = \sum_{\alpha=-1}^{1} w_{P(i+\alpha, j+1)} D_{i+\alpha, \, j+1} +$$

$$\sum_{\alpha=-1}^{1} w_{P(i+\alpha, j)} D_{i+\alpha, \, j} + \sum_{\alpha=-1}^{1} w_{P(i+\alpha, j-1)} D_{i+\alpha, \, j-1}. \tag{16}$$

Using (14) and (15A) the first sum in (16) is

$$2\Delta \sum_{\alpha=-1}^{1} w_{p(i+\alpha, j)} D_{i+\alpha, j+1} =$$

$$w_{P(i-1, j+1)} \left[\sum_{p=1}^{N_{i,j+1}} w_p h_p - \sum_{p=1}^{N_{i-2, j+1}} w_p h_p \right] + w_{P(i, j+1)} \left[\sum_{p=1}^{N_{i+1, j+1}} w_p h_p - \sum_{p=1}^{N_{i-1, j+1}} w_p h_p \right]$$

$$+ w_{P(i+1,, j+1)} \left[\sum_{p=1}^{N_{i+2, j+1}} w_p h_p - \sum_{p=1}^{N_{i, j+1}} w_p h_p \right].$$

Now, h_P does not appear in the $N_{i-2, j+1}$ and $N_{i+2, j+1}$ sums since P is not in either cell. It also appears once in each of the other four sums; however, the terms exactly cancel. It is readily seen that this is true for each of the other sums in (16) as well as the y component of the gradient.

The cancelation of particle height in the interpolated gradient to a particle is analogous to the condition that second order accurate finite differences at grid points do not depend on the value of the function at those grid points. The importance of this to the present application is that there is no self-induced motion of a particle. This result arises for two reasons. First, the same weights are used for the interpolation from particles to the grid and then back to the particles and not because of a specific form such as (12). Second, the order of accuracy of the derivative (second order in our case) is not higher than that of the interpolation routine. Fourth order accurate derivatives used in conjunction with a lower order interpolation scheme may produce self motion and thus would not be as accurate as the second order schemes.

This method has several other attributes. First, the weights are computationally efficient since they are not difficult to calculate and are used both for interpolation from particles to grid points and back to the particles. Second, (9) is automatically satisfied since the heights and volumes of the particles are assigned initially and are fixed. Moreover, it is not necessary to interpolate particle velocities as long as there is no viscosity in the problem. Finally, any stable time integrator can be used to advance the position each particle.

The major tradeoff in choosing the integrator is that between accuracy and computational work. For example, a two step integrator, such as a second order Runge-Kutta scheme, has an accuracy of $O((\delta t)^2)$ but requires two evaluations of ∇h at each particle. Thus this integrator would require two interpolations of the particle heights to the grid, two applications of the finite difference form of ∇ to h on the grid and two interpolations of ∇h to the particles for each position advancement. On the other hand a first order accurate integrator with a much smaller time step could provide the same degree of accuracy with less computation per time step.

2.3 Initialization of Height Field

We shall illustrate this method in the next section by an application to an initially circular lens. For initial conditions we choose a parabolic lens that has been the subject of considerable study [18, 20 – 35]. In these studies the lens velocity and thickness were specified as

$$h = h_o(t) + B_{ij}(t)x_i x_j, \quad \text{for } h \geq 0$$

$$v_i = G_{ij}(t)x_j, \quad \text{for } h \geq 0$$

$$v_i = 0, \quad \text{elsewhere} \tag{17}$$

Here the summation convention is used for repeated indices and the spatial coordinate x_i is measured from the center of mass of the lens. Note that the velocity field is discontinuous

at $h = 0$ as is ∇h. Moreover, the discontinuous frontal boundary, $h = 0$ must be calculated as part of the solution. Conventional gridded methods are not well suited for problems of this sort.

Substitution of (17) into (8) and (9) yields 8 coupled nonlinear ordinary differential equations for $G_{ij}(t)$, $h_o(t)$ and $B_{ij}(t)$. As shown in [24] and [34] the resulting solutions can be represented as a nonlinear superposition of rotational, deformational and horizontal divergence modes. The lens frontal boundary generally may oscillate between a circle and an ellipse which tends to rotate anticyclonically. Particle motion can be quite complicated; see for example sample trajectories in [31]. Solutions based on (17) will be called lens solutions.

The nondimensional equation for the initial lens thickness is

$$h = h_o[1 - (r/R)^2], \tag{18}$$

where h_o is the centerline thickness, r is the radial coordinate from the lens center and $R = [|B_{11} + B_{22}|/2]^{-1}$ is the radius of the lens. The volume occupied by the lens is

$$V_L = 2\pi \int_0^R rh\,dr = (\pi/2)h_o R^2. \tag{19}$$

Integration of (11) shows the volume of a particular particle to be $V_p = \Delta^2 h_p$ so the total volume occupied by the particles is

$$V_T = \Delta^2 \sum_{p=1}^N h_p, \tag{20}$$

where N is the total number of particles. Clearly, $V_T = V_L$ must be required.

Consider first the case where h_p is the same for all particles. Then,

$$N = V_T/V_p = (\pi/2)(h_o/h_p)(R/\Delta)^2. \tag{21}$$

To estimate N, divide the lens into concentric circular annuli surrounding an axial cylinder centered at the lens center. The radial width of an annulus is $2\Delta/d$ with $d \geq 2$, and the

height of the lens along the axis of an annulus is given by (18). In the limiting case, $d = 2$, the annulus width is the same as the computational cell discussed in the previous section. Since the annuli are used for the initial distribution of particles in the lens it is appropriate to have the annuli spacing finer than that of the computational cells.

The axis of the outermost annulus is at radius $r = R - \Delta/d$. Then the height along this axis is

$$h_L = h_o(\Delta/Rd)(2 - \Delta/Rd). \tag{22}$$

Obviously, $h_p \leq h_L$ with the equality holding for just one particle in each cell on the lens boundary. Using this limiting case for h_p in (21) gives

$$N = (\pi/2)(R/\Delta)^3 d/(2 - \Delta/Rd). \tag{23}$$

All having the same height, these particles must be distributed nonuniformly in the lens. We shall use $R = 10^{-1}$, $\Delta = 4 \times 10^{-3}$ and $d = 16$ so (23) suggests $N \sim O(2.5 \times 10^5)$ for $h_p \sim h_L$. However, requiring ten particles in each cell in the outer boundary increases N by an order of magnitude.

The number of particles can be reduced by decreasing the horizontal resolution; i.e., increasing Δ/R. From (23) it is seen that changes in resolution can cause dramatic changes in the particle count. An order of magnitude change in resolution produces three orders of magnitude change in the number of particles.

One of the problems that arises with a constant h_p is that the number of particles in each cell will vary with radius with fewer particles in the outermost cells. This can be overcome by allowing h_p to vary with radius as well. The volume of an annulus centered at r is

$$V_A = 2\pi \int_{r-\Delta/d}^{r+\Delta/d} rhdr = 4\pi h_o r(\Delta/d)[1 - (r/R)^2 - (\Delta/Rd)^2].$$

The number of particles required to fill this volume is

$$N_A = V_A/V_p = 4\pi[h_o/h_p(r)](r/\Delta d)[1 - (r/R)^2 - (\Delta/Rd)^2]. \tag{24}$$

The number of cells in this annulus is the ratio of the annulus area to cell area. A simple calculation gives this number as $N_c = 4\pi r/\Delta d$. If the number of particles in each cell, $N_\# = N_A/N_c$, is to be constant the particles heights must be distributed as

$$h_p(r) = (h_o/N_\#)[1 - (r/R)^2 - (\Delta/Rd)^2]. \tag{25}$$

Adjusting the height of the particles to keep the number of particles in a cell constant also changes the requirements on the total number of particles. The cross-sectional area of the lens annulus is $\pi[R^2 - (\Delta/d)^2]$. Thus, the number of cells needed to cover the lens annulus is

$$N_{\text{cell}} = \pi[R^2 - (\Delta/d)^2]/\Delta^2, \tag{26}$$

and the total number of particles in the lens annulus is

$$N_{TA} = N_\# \cdot N_{\text{cell}}. \tag{27}.$$

To complete this analysis it is necessary to fill the inner cylindrical core. Its volume is

$$V_I = 2\pi \int_0^{\Delta/d} rhdr = \pi h_o(\Delta/d)^2[1 - (1/2)(\Delta/Rd)^2]. \tag{28}$$

The number of particles required to fill this void is

$$N_I = \pi[h_o/h_{p(I)}d^2][1 - (1/2)(\Delta/Rd)^2]. \tag{29}$$

This is determined by an arbitrary choice of $h_{p(I)}$. Here we use $N_I \sim 10^3$.

A critical issue with this approach is an appropriate number of particles for each cell $N_{\#}$. Using different particle geometry than we do, other investigators [13 – 15] used about 15 particles per cell. It should be noted that these investigators used smoothing at every timestep. With our geometry and elimination of smoothing it appears that $N_{\#} \sim 5 \times 10^2$ is required for reasonable resolution and accuracy.

With $N_{\#} \sim 5 \cdot 10^2$ the total number of particles is

$$N_T = N_{TA} + N_I \sim 10^6. \tag{30}$$

Finally, it should be noted that we use a polar coordinate system here *only* to initialize the distribution of particles. The calculations presented in the next section are done with a rectangular grid even for those problems which exhibit radial symmetry.

3   APPLICATION TO AN ISOLATED LENS

The first simulation discussed here was designed to test the ability of the PIC ansatz to reproduce, with small phase error and amplitude distortion, a single frequency in a nonlinear flow and to provide high resolution of the associated oscillating front. Here and in the next problem we shall use the variable height formulation. It is stressed that there is no smoothing in the results presented below other than what occurs with the interpolation.

As a control for the PIC simulation, comparisons will be made with numerical solutions of the lens model. In the latter model the height field is parabolic and the velocity field linear with respect to the distance from the lens center for all time. These constraints are imposed only initially on the PIC model. In both cases a second order accurate Runge-Kutta integrator was used.

The initial velocity field for the PIC model was taken as the same as the lens model; i.e.,

$$v_1(0) = (G/2)x_1 - (G_R)x_2,$$

$$v_2(0) = (G_R)x_1 - (G/2)x_2, \tag{31}$$

where $G = G_{11}(0) + G_{22}(0)$ is the initial horizontal divergence and $G_R = [G_{12}(0) - G_{22}(0)]/2$ is the initial spin. Numerical values for this experiment are given in the table.

For the lens model [21] obtained an analytic solution for h_o, B_{ij} and G_{ij}, which is called here the pulson solution. The nondiagonal components of B_{ij} and the symmetric component of G_{ij} are zero for all time while the remaining components as well as h_o oscillate at the Coriolis frequency f. Unlike most nonlinear problems the oscillation frequency of the pulson is independent of the initial conditions. Of particular interest here are the analytic expressions for the centerline height, h_o, and $[|B_{11} + B_{22}|/2]^{-1}$ since these two variables determine the height field and the evolution of the lens boundary. These are found to be

$$h_o(t) = H\Gamma(t),$$

$$h(t) = h_o(t) - (\Lambda_B/4)\Gamma^2(t), \tag{32}$$

where H is the layer thickness scale at $t = 0$, Λ_B is given by the initial conditions of $B_{11} + B_{22}$ and

$$\Gamma(t) = [A + \gamma \sin ft]^{-1}, \quad A > |\gamma|.$$

Also, A and γ are given by initial conditions of G_{ij}.

Figure 4 shows typical trajectories for the PIC (solid curve) and lens solutions (dashed curve). Both particles start at same initial position shown as a triangle and both exhibit the same cycloidal behavior characteristic of this solution. The boxes show the position at one day intervals. This motion is composed of general anticyclonic rotation about the lens center with small loops at the inertial frequency. As seen in panel a, the trajectories are virtually

18

identical for the first 1.5 days; however, by day 2 some offset is apparent. Although there is some growth in the offset it is mostly completed by day 5 as seen in the starting and ending offsets in panel b. The PIC solution exhibits some irregularity in the spacing of the inertial loops. The period, however, is very nearly inertial as expected.

Figure 5 compares the PIC solution for the centerline height h_o (solid curves) with the analytic solution given by (32). This figure shows that the PIC solution accurately reproduces both the amplitude and phase of the analytic solution. Figure 6 compares the PIC height field after 10 days (solid curve) with the initial height field. Because the solution is periodic, these fields should be identical. Again, the comparison is excellent although there is some indication that near the lens center the PIC simulation is slightly thinner than the exact solution. This is also reflected in the slight increase in the simulation thickness at mid radii. The difference between the initialized field for PIC and the analytic solution could not be seen at normal plotting scales.

The above flow field had vorticity and horizontal divergence but no deformation. To test the efficacy of the PIC model in the presence of a time dependent deformation component of the velocity field, the initial velocity (31) was replaced by

$$v_1(0) = (G/2 + G_N)x_1 + (G_N - G_R)x_2,$$

$$v_2(0) = (G_N + G_R)x_1 + (G/2 - G_N)x_2. \tag{33}$$

Here $G_N = [G_{11}(0) - G_{22}(0)]/2$ is the initial normal deformation and $G_S = [G_{12}(0) + G_{21}(0)]/2$ is the initial shear deformation. Numerical values are given in the table.

The solution for the lens case was obtained by numerically integrating the eight equations for h_o, B_{ij} and G_{ij}. See [31] and [33] for details regarding the solution procedure. This solution shows that the lens boundary starts as a circle, quickly deforms into an ellipse

19

which rotates anticyclonically for a brief period then abruptly deforms back to a circle. This cycle is repeated; however, each new repetition of the circular or ellipse phase does not have the same geometric characteristics as the previous phase.

Figures 7 and 8 show the evolution of two example trajectories. Figure 7 is typical of trajectories for particles started near the lens center. This figure shows that the trajectory for the lens model particle tends to stay near the center although there is considerable irregularity in the trajectory. In contrast the PIC particle tends to wander away from the lens center. This is consistent with the results of the previous experiments. Other than exhibiting anticyclonic rotation the two trajectories appear uncorrelated at very early time.

Figure 8 shows typical paths for particles started near the initial lens boundary. Here the trajectories from the PIC and lens model are in good agreement for the first two days. Thereafter the trajectories exhibit only crude similarities such as anticyclonic rotation and cycloidal looping. As with the previous experiment, the lens model trajectory shows greater excursions from the lens center than does the PIC model.

Figure 9 compares the PIC centerline height (solid curve) with the numerical solution to the lens model. As seen in this figure, the solutions agree quite well through day 2. After this time the solutions agree well in phase but the amplitude of the PIC solution tends to be slightly smaller than the lens solution. This is consistent with the indication from Fig. 7 that with the PIC solution the lens tends to flatten.

Figures 10 and 11 compare the evolution of the lens boundary determined by the PIC model with the lens solution. The detailed evolution for the first day is shown in figure 10 while figure 11 shows snapshots of the boundary over a 10 day period. It is seen in these figures that up to day 2.5 the PIC and lens solutions are in close agreement. Both quickly evolve to an elongated ellipse which rotates anticyclonically. At day 2.5 the boundary has evolved to a more circular shape. Thereafter the PIC solution continues to display an elliptical mode; however it is not nearly as pronounced as that of the lens solution. By day

8 there is some indication of a Kelvin-Helmholtz type instability at the boundary of the PIC solution; however, the growth rate does not seem large.

The discrepancies between the two model simulations begin around day 2. There is no indication of numerical instability in either case and no indication of a hydrodynamic instability in the PIC simulations other than a possible weak Kelvin-Helmholtz instability late in the simulation. Note that hydrodynamic instabilities are precluded by the formulation of the lens model since the height and velocity profiles are required for all time to be parabolic and linear respectively. Thus either solution could be representative of real oceanic lenses. Since the PIC model has fewer restrictions we prefer it.

The PIC calculations described above used approximately 10^6 particles. In order to illustrate the deterioration in the solution when less particles are used the deformation case was repeated with only about 10^5 particles. Figure 12 shows the evolution of the centerline height for the two cases. It is seen that the peaks and troughs become ragged for the reduced particle case. Note that for plotting purposes the 10^6 particle case is shown as the dotted curve while the 10^5 particle case is shown as the solid curve.

4   CONCLUSIONS

The results presented in the previous section are very encouraging. The comparison of the simulations and the pulson analytic solution showed that the PIC method used here was able to reproduce both the amplitude and phase of the analytic pulson solution with negligible distortion. The case of the deforming vortex provided a good test of the method for handling typical evolutions of fronts in which local horizontal divergence, vorticity and deformation are all important. The time and space scales of the front oscillations would be computationally costly to treat by conventional gridded primitive equation models. The agreement between the PIC simulations and the numerical results from the lens model indicate that the former is capable of treating problems with dynamically evolving interfaces.

21

The formulation used here allows for the particles to interpenetrate so that a given spatial position generally will be contained within the volumes of many particles. This means that with this formulation it is not appropriate to consider material properties as characteristic of a single particle occupying a particular position at a particular time. Rather material properties should be viewed as a suitable weighted average of all the particles influencing the position at the particular time.

It is noteworthy that the results achieved here did not require any smoothing other than that implicitly contained in the interpolation and differentiation operations. Perhaps this is due to our choice of the particle shape and weighting. This approach may be better suited to simulating a continuous fluid media than schemes which use simpler shapes and weighting functions.

There are still unresolved issues regarding the utility of this approach, however. No one has yet introduced a fully dynamically interacting lower layer. By prescribing a quasi-geostrophic response in the lower layer [16] was able to use conventional gridded methods for obtaining the solution in that region while using PIC methods in the upper layer. Using PIC methods in both layers should be quite challenging. Another question is to determine how well the method treats streaming flows. In this case the particles are advected out of one part of the domain and must be replaced by inflow from another part. There is no experience with PIC methods in a geophysical fluid dynamics setting with problems of this sort. Finally, it will be important to consider surface stress-driven flow and flow over topography. In these cases it will be necessary to incorporate viscosity, which will require some modifications in the approach used here.

References

[1] M. Olim. *J. Comput. Phys.*, **112**, 253, 1994.

[2] J. P. Christiansen. *J. Comput. Physics*, **13**, 363, 1973.

[3] J. P. Christiansen and N.J. Zabusky. *J. Fluid Mech.*, **61**, 219, 1973.

[4] J. K. Dukowicz and B. Meltz. *J. Comput. Phys.*, **99**, 115, 1992.

[5] G. S. Winckelmans and A. Leonard. *J. Comput. Phys.*, **109**, 247, 1993.

[6] G. Russo. *J. Comput. Phys.*, **108**, 84, 1993.

[7] F. H. Harlow. *Meth. Comput. Physics*, **3**, 319, 1964.

[8] F. Brunel, J. N. Leboeuf, T. Tajima, and J. M. Dawson. *J. Comput. Phys.*, **43**, 28, 1981.

[9] J. U. Brackbill and H. M. Ruppel. *J. Comput. Phys.*, **65**, 314, 1986.

[10] P. J. O'Rourke, J. U. Brackbill, and B. Larrouturou. *J. Comput. Phys.*, **109**, 37, 1993.

[11] N. J. Zabusky and J. C. McWilliams. *Phys. Fluids*, **25**, 2175, 1982.

[12] S. B. Hooker. PhD thesis, University of Miami, Miami, Florida, 1987.

[13] E. G. Pavia and B. Cushman-Roisin. *J. Geophy. Res.*, **93**, 3554, 1988.

[14] E. G. Pavia and B. Cushman-Roisin. *J. Phys. Oceanog.*, **20**, 1886, 1990.

[15] E. G. Pavia. PhD thesis, Florida State University, Gainesville, Florida, December 1989.

[16] B. J. Mathias. Master's thesis, Thayer School of Engineering, Dartmouth College, New Hampshire, April 1992.

[17] H. E. Hurlburt and J. D. Thompson. *J. Phys. Oceanog.*, **3**, 16, 1973.

[18] B. Cushman-Roisin, W. H. Heil, and D. Nof. *J. Geophy. Res.*, **90(C6)**, 11,756, 1985.

[19] R. W. Hockney and J. W. Eastwood. Computer Simulation Using Particles. Institute of Physics, 1992.

[20] G. R. Goldsbrough. In *Proc. R. Soc. London*, **A30**, 157, 1930.

[21] F. K. Ball. *J. Fluid Mech.*, **19**, 240, 1963.

[22] F. K. Ball. *J. Fluid Mech.*, **22(3)**, 529, 1965.

[23] W. C. Thacker. *J. Fluid Mech.*, **107**, 499, 1981.

[24] W. R. Young. *J. Fluid Mech.*, **171**, 101, 1986.

[25] B. Cushman-Roisin. *Tellus*, **39(A)**, 235, 1987.

[26] P. Ripa. *J. Fluid Mech.*, **183**, 343, 1987.

[27] B. R. Ruddick. *J. Phys. Oceanog.*, **17**, 741, 1987.

[28] C. Rogers. *Phys. Lett. A*, **138**, 267, 1989.

[29] D. Brickman and B. Ruddick. *J. Geophy. Res.*, **95**, 9657, 1990.

[30] A. D. Kirwan, Jr., A. W. Indest, J. Liu, and N. Clark. *J. Geophy. Res.*, **95**, 18,057, 1990.

[31] A. D. Kirwan, Jr. and J. Liu. In A. R. Osborne, editor, *Nonlinear Topics in Ocean Physics*, Course CIX, pages 99–132, North Holland, Amsterdam, 1991. International School of Physics, 'Enrico Fermi'.

[32] T. Kawano and S. Nakamoto. *J. Geophy. Res.*, **97**, 12,659, 1992.

[33] A. D. Kirwan, Jr., B. L. Lipphardt, Jr., and J. Liu. *Inter. J. Eng. Sci.*, **30(10)**, 1361, 1992.

[34] A. D. Kirwan, Jr., B. L. Lipphardt, Jr., and K. L. Gregory. In S.K. Majumdar, E. W. Miller, G. S. Forbes, R. F. Schmalz, and A. A. Panah, eds., *The Oceans: Physical-Chemical Dynamics and Human Impact*. The Pennsylvania Academy of Sciences, 1994.

[35] A. D. Kirwan, Jr. and B. L. Lipphardt, Jr. *J. Mar. Sys.*, **4(2-3)**, 95, 1993.

Table: Initial Conditions

	Pulson Case	Deformation Case
h_o	4.875×10^{-4}	4.875×10^{-4}
$(B_{11} + B_{22})/2$	-9.75×10^{-2}	-9.75×10^{-2}
$B_{12}, \ B_{21}$	0	0
G_R	-0.25	-0.25
G_N	0	0.2
G_S	0	0.1
G	0.6	0.6

Figure Captions

Figure 1 Cartoon of the two layer model.

Figure 2 Perspective picture of the shape of a particle.

Figure 3 Cross section of a particle along the x axis. The hatched, open, and cross-hatched areas divided by Δ give the weights specified in (12). The two vertical dashed lines are the cell boundaries.

Figure 4 Typical trajectories for the PIC (solid curve) and lens model (dashed curve) for the pulson case. The triangle is the starting point for both trajectories and the boxes give the positions at one day intervals. Panel a shows the first five days and panel b the last five days of the simulation. The dotted line in panel a gives the initial lens boundary.

Figure 5 Comparison of the PIC centerline height with the analytic solution for the pulson case. The PIC result is the solid curve and the analytic solution is the dashed curve.

Figure 6 Comparison of h at $t = 10$ days from the PIC model (solid contours) with the initial h (dashed contours) for the pulson case.

Figure 7 Typical trajectories for the PIC (solid curve) and the lens model (dashed curve) for particles starting near the origin for the deformation case. Panel a is for the first five days and panel b is for the last five days of the simulation. The symbol convention is the same as in Figure 4.

Figure 8 Typical trajectories for the PIC (solid curve) and the lens model (dashed curve) for particles starting near the initial lens boundary for the deformation case. Panel a is for the first five days and panel b is for the last five days of the simulation. The symbol convention is the same as in Figure 4.

Figure 9 Comparison of the PIC centerline height with the numerical solution to the lens model over 10 days for the deformation case. The PIC solution is the solid curve while the lens solution is the dashed curve.

Figure 10 Comparison of the evolution of the lens boundary determined by the PIC model with that of the lens model over 1 day for the deformation case. The PIC solution is the solid curve while the lens solution is the dashed curve.

Figure 11 Comparison of the evolution of the lens boundary determined by the PIC model with that of the lens model over 10 days for the deformation case. The PIC solution is the solid curve while the lens solution is the dashed curve.

Figure 12 Comparison of the centerline height evolution for PIC simulations with approximately 10^6 particles (dotted curve) and 10^5 particles (solid curve) for the deformation case.
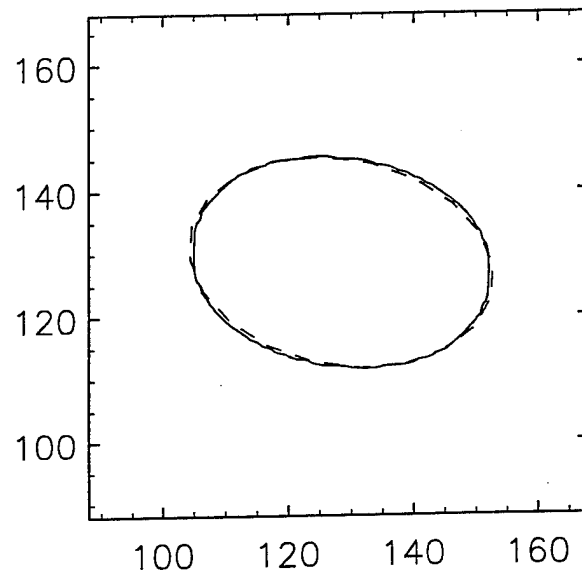
y   z   x

h_1

h_2

Fig.
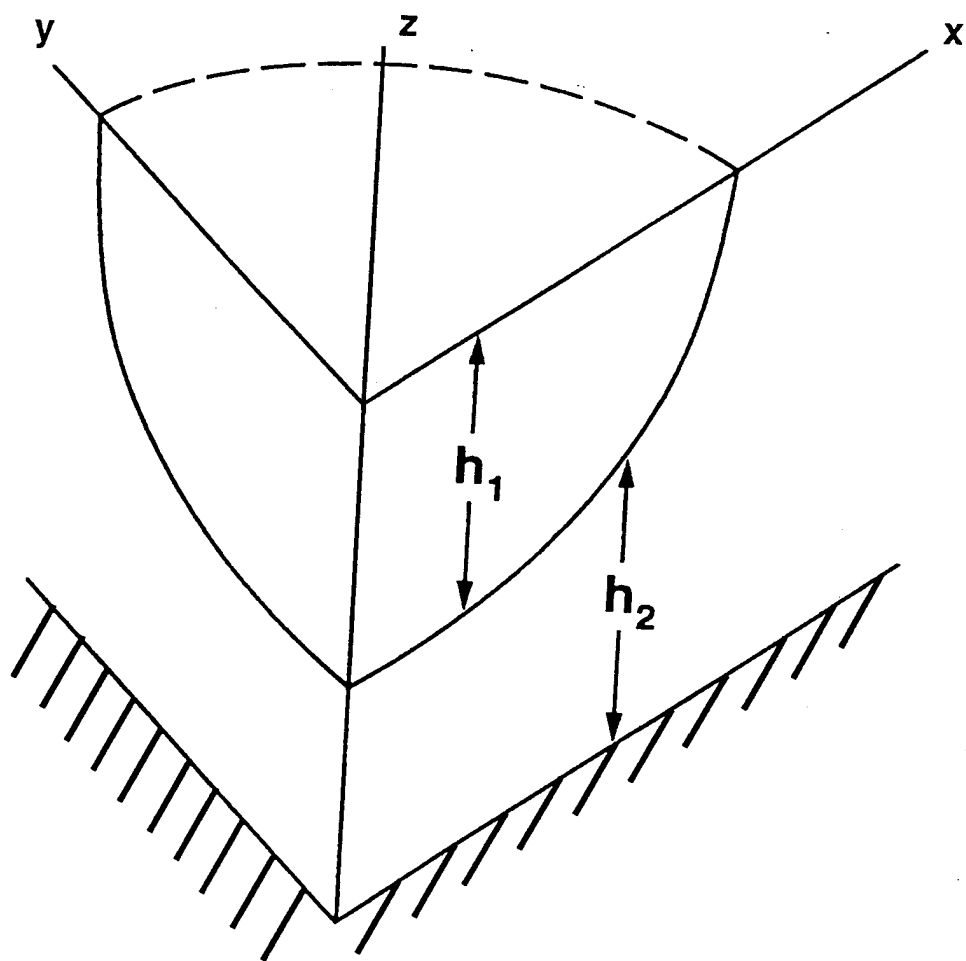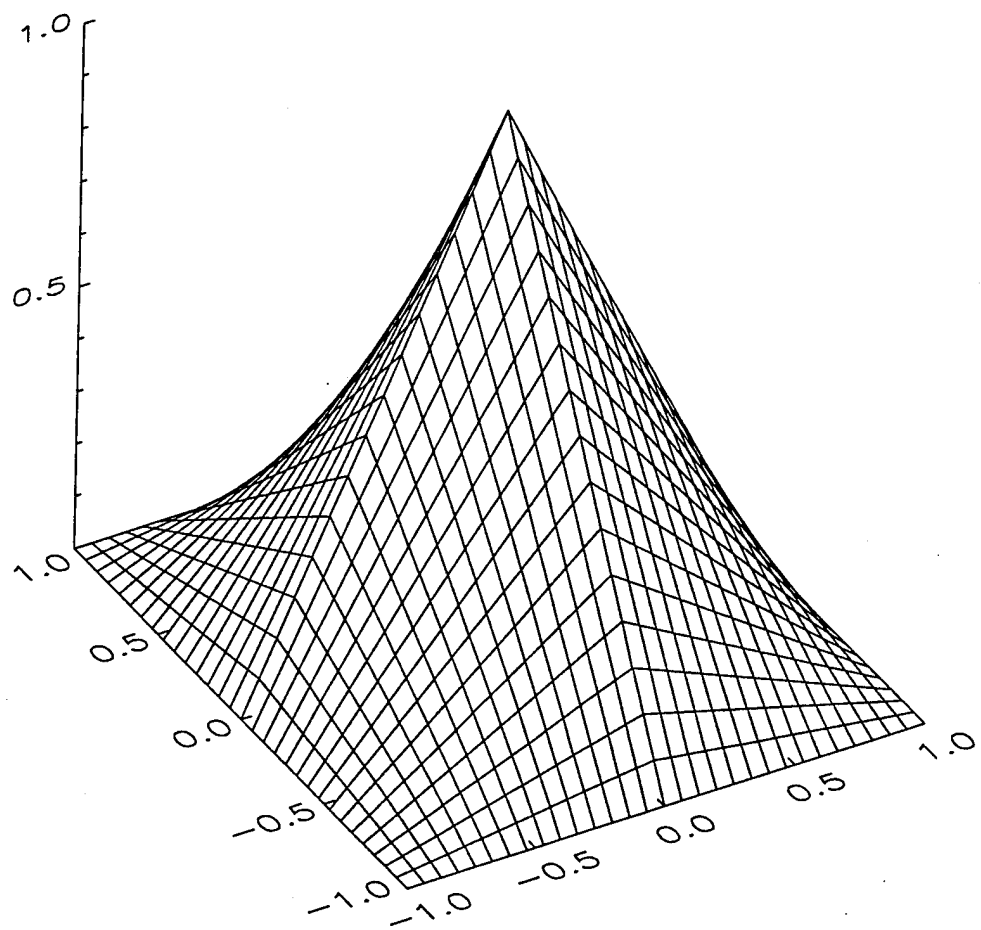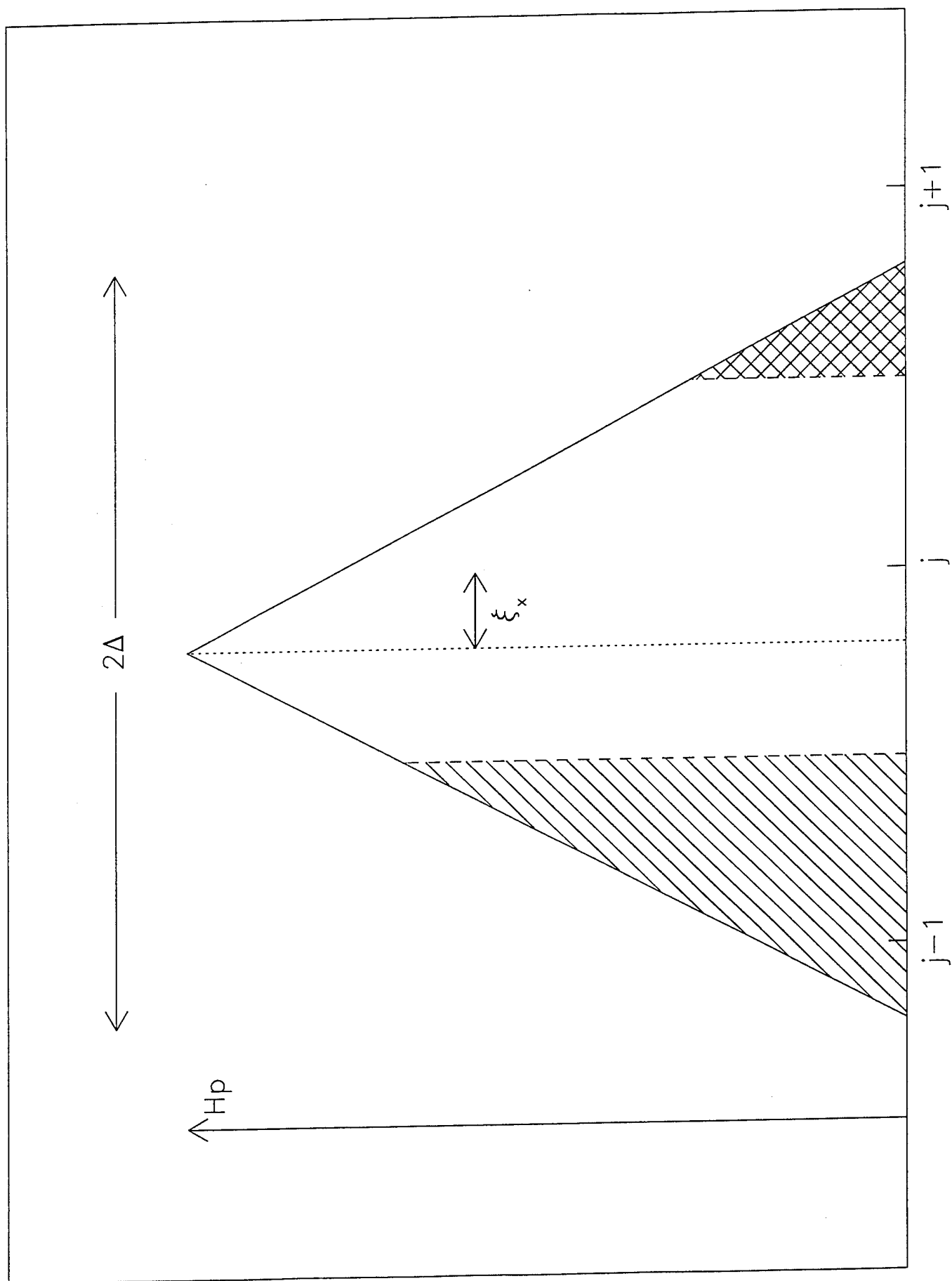
Fig 3
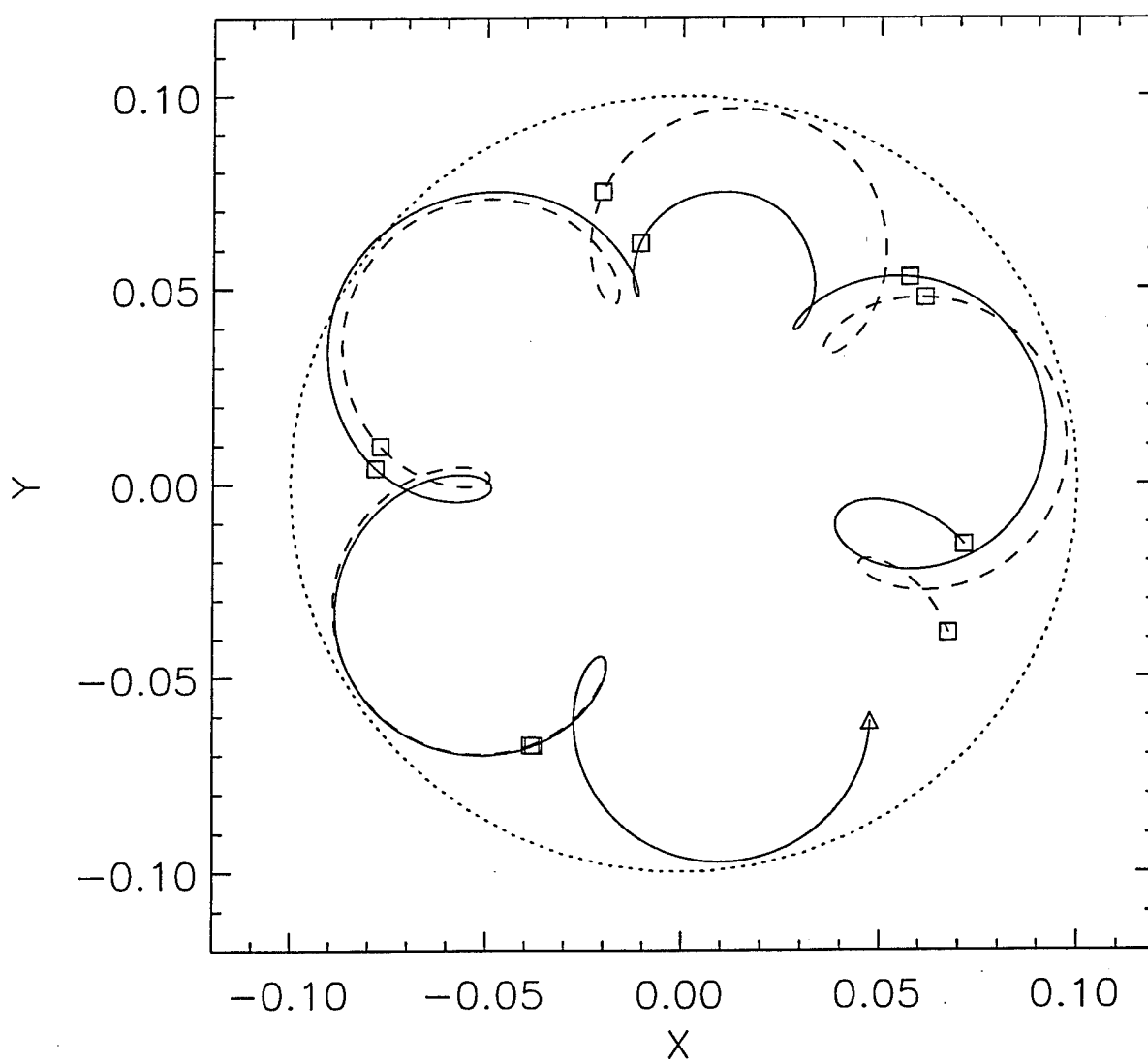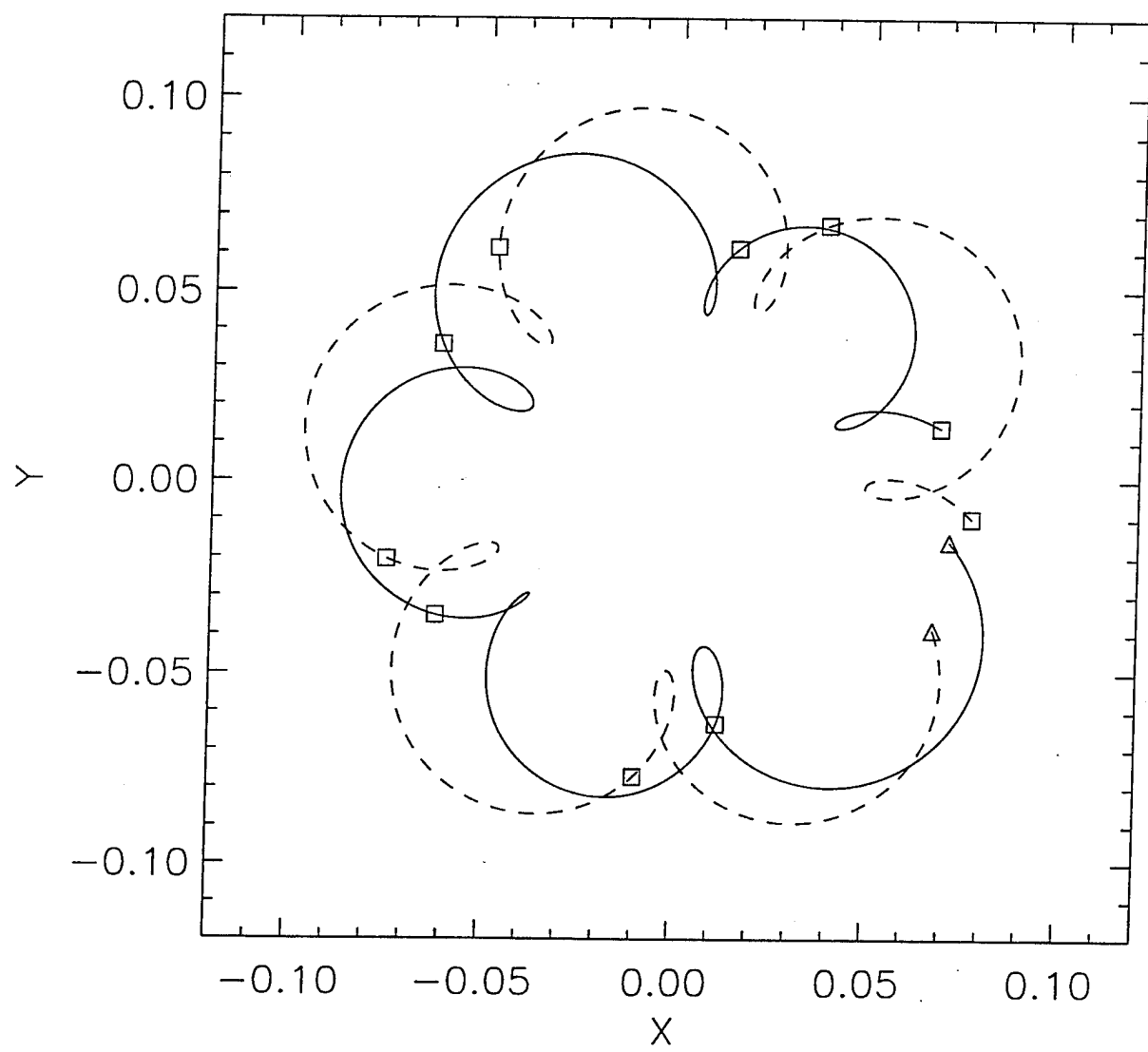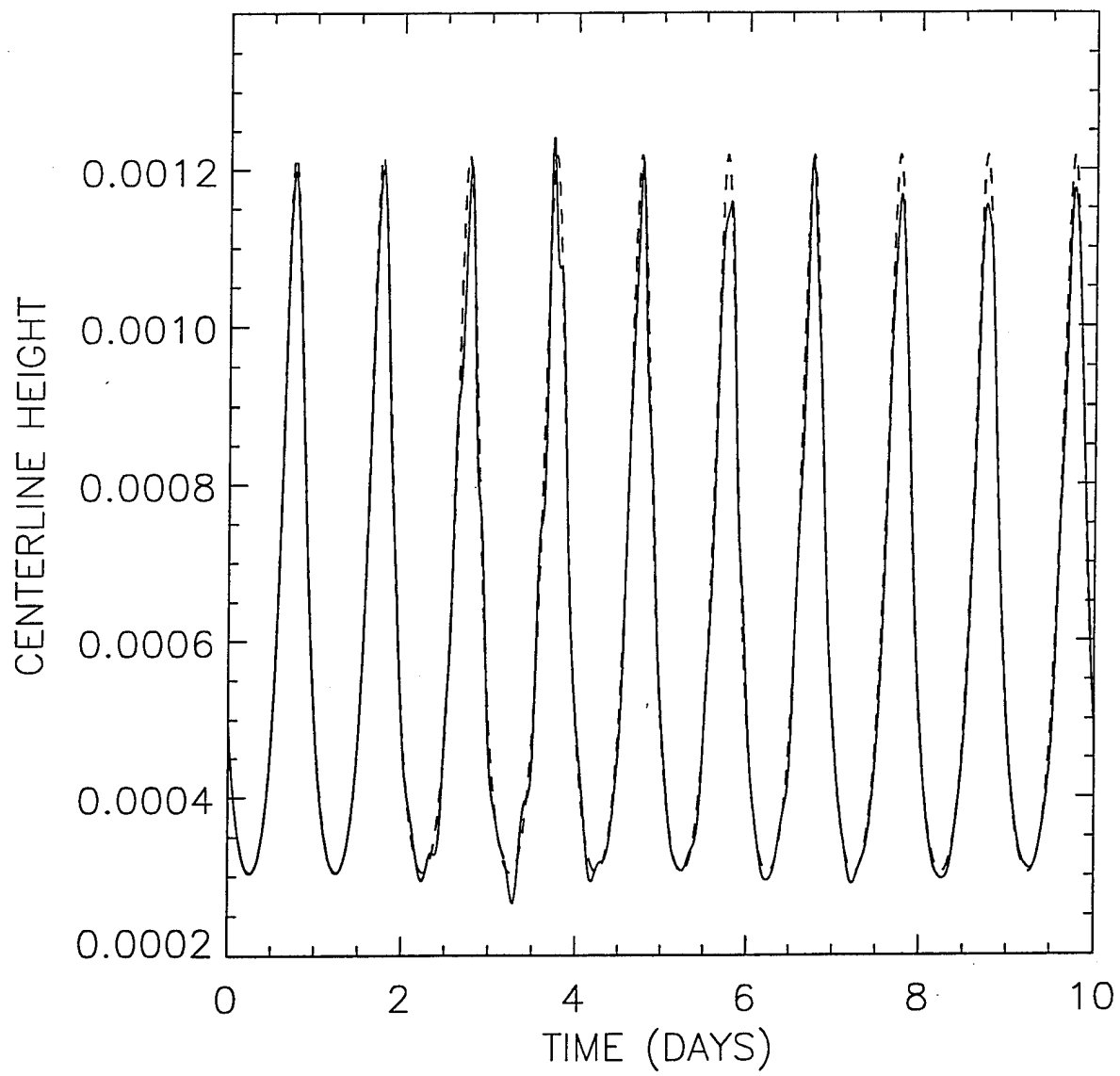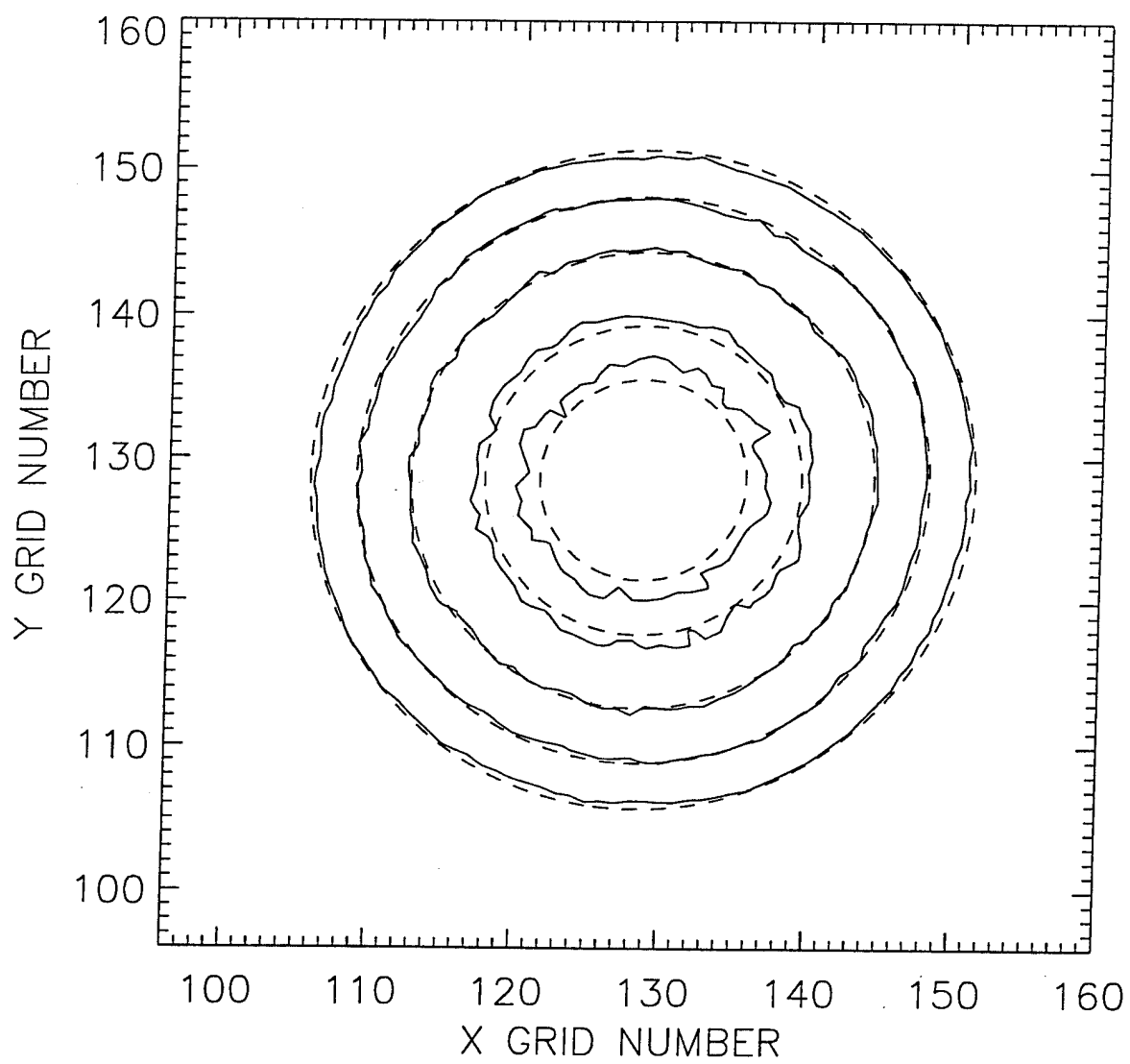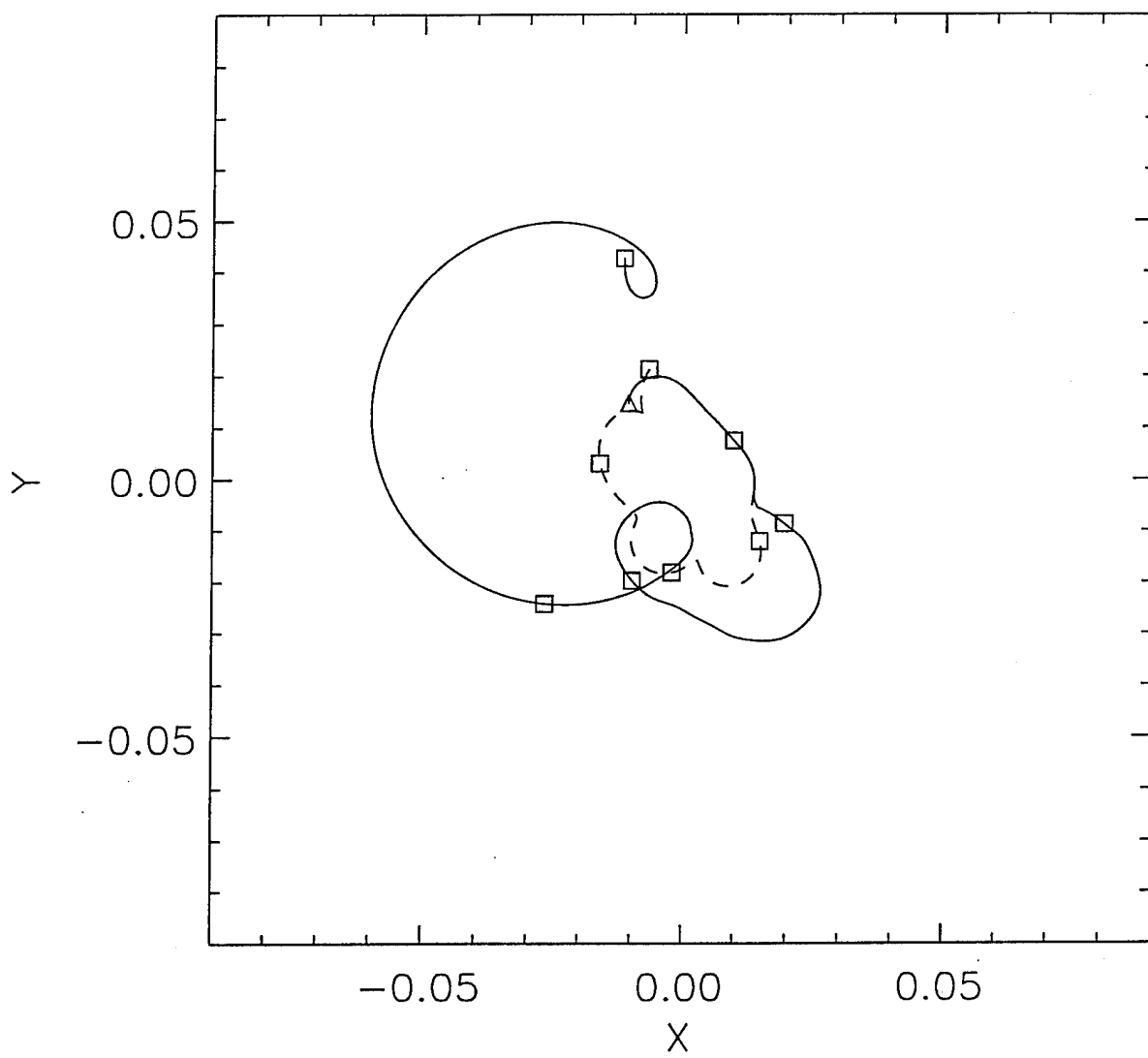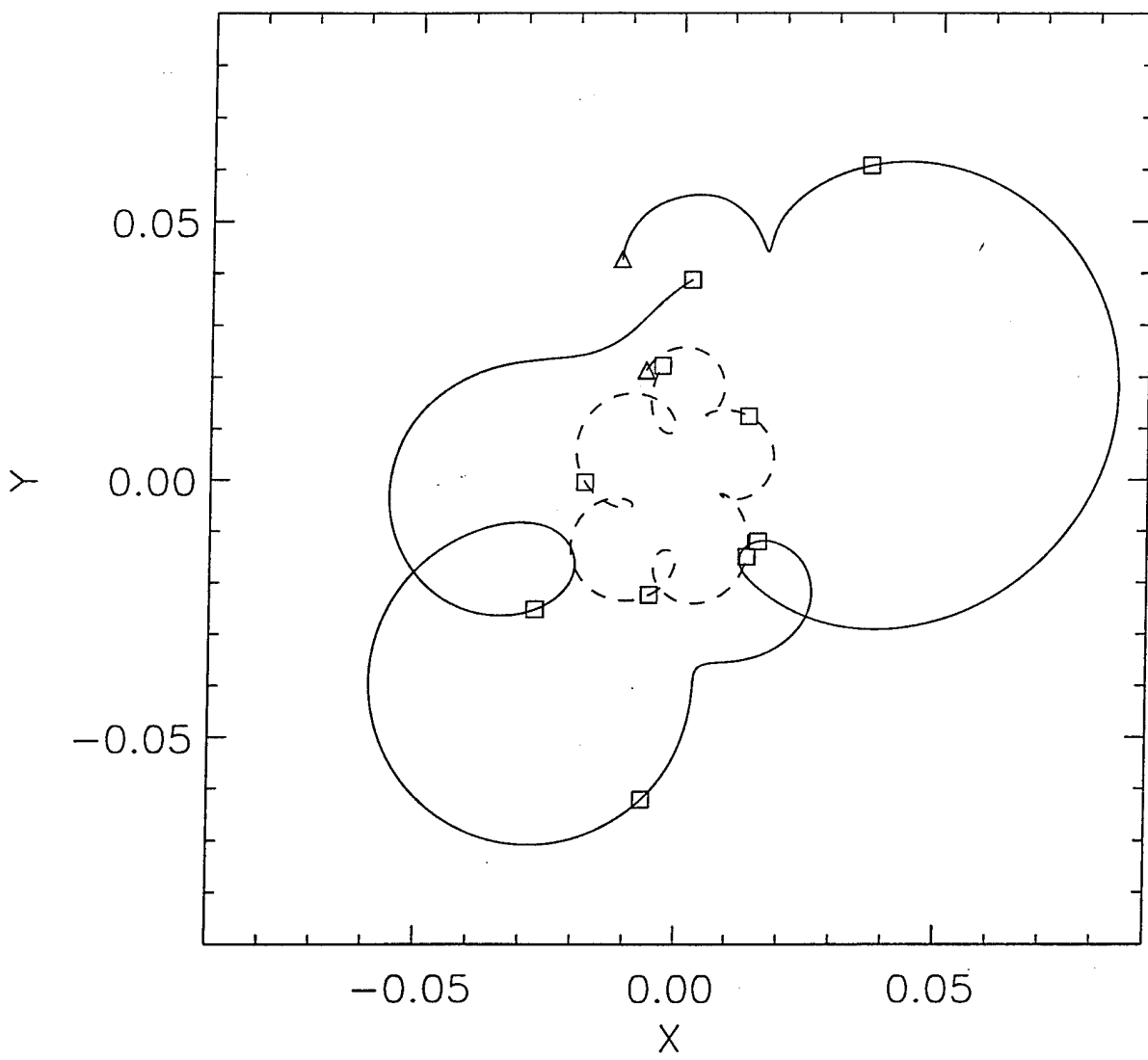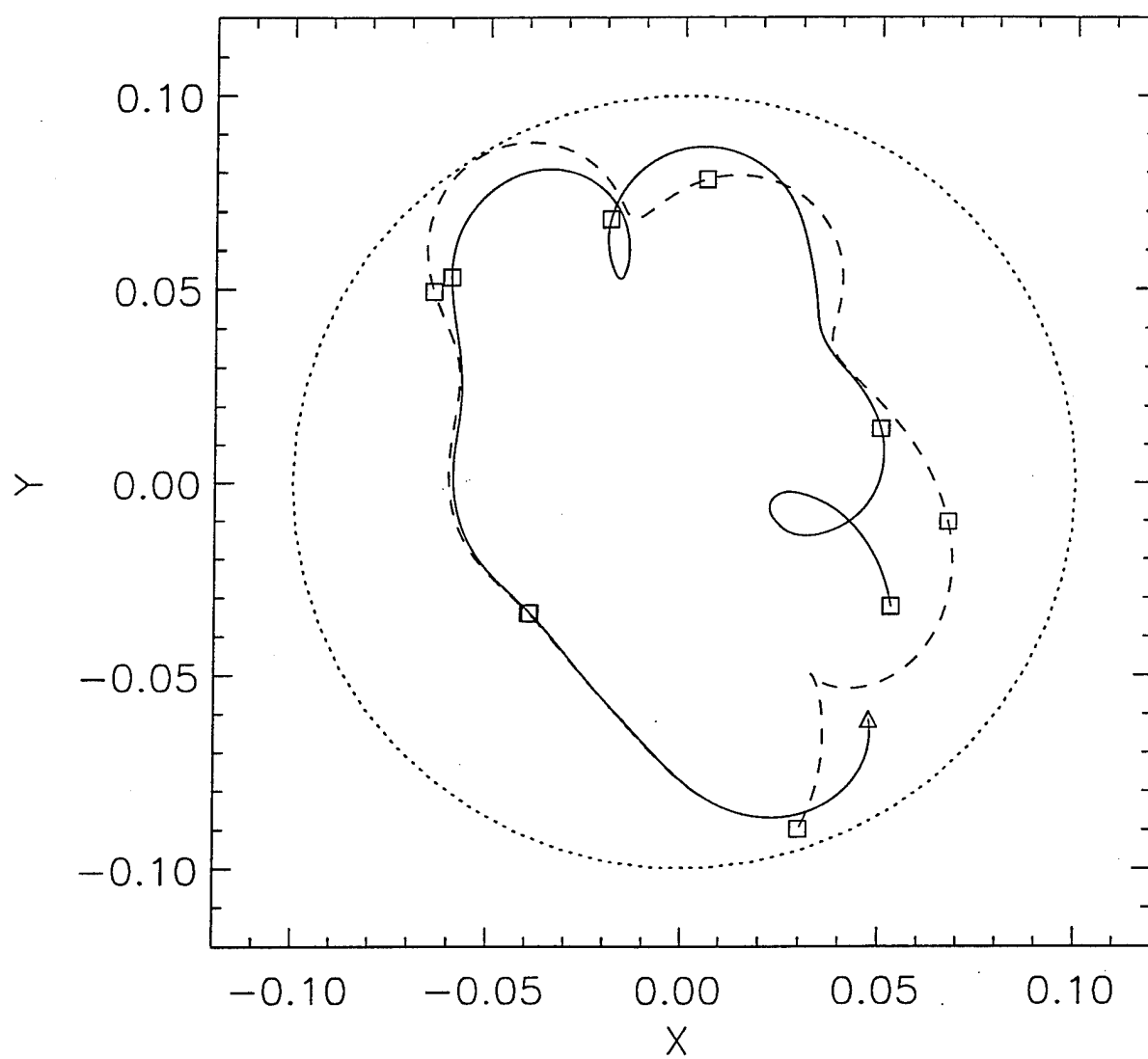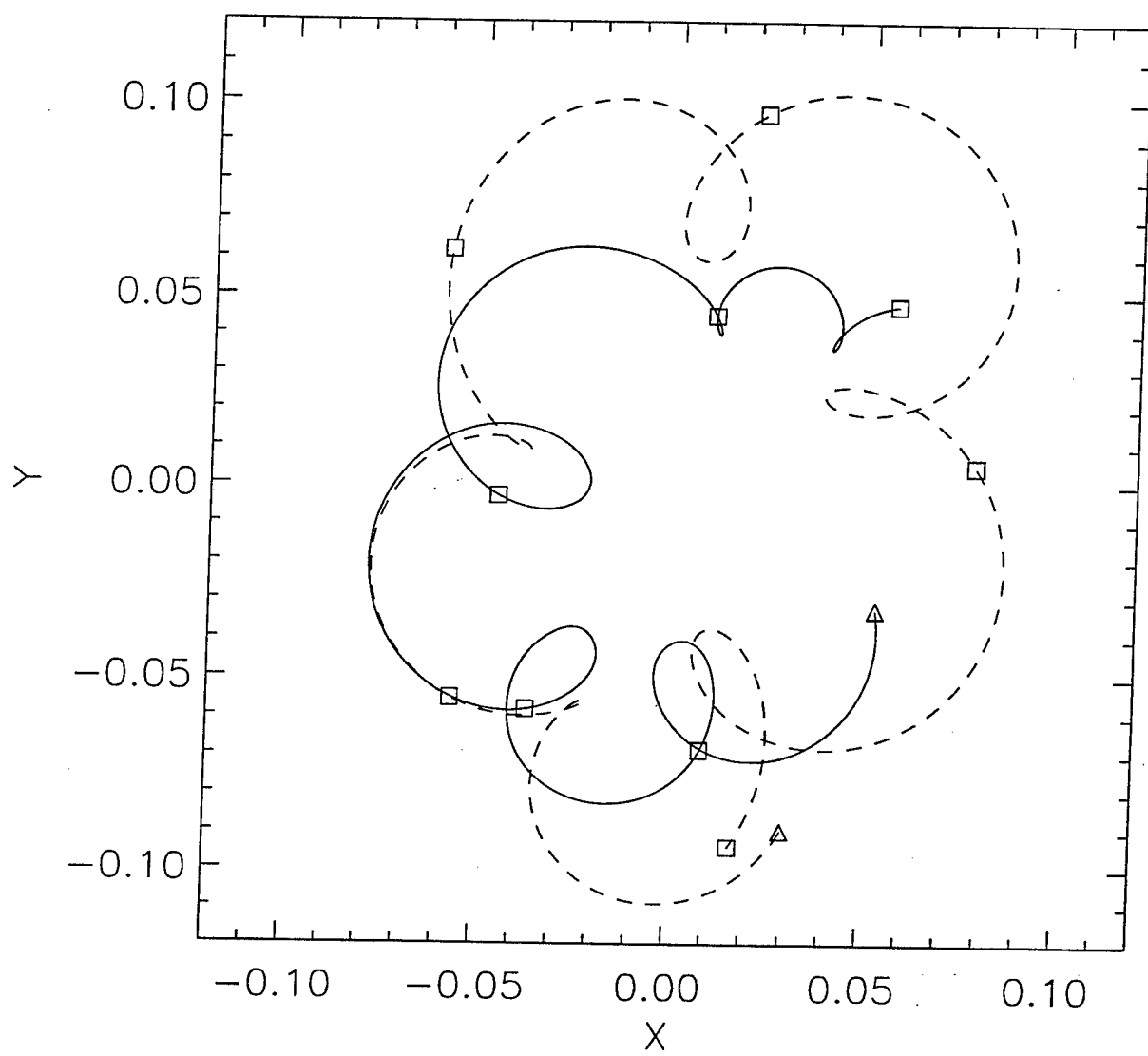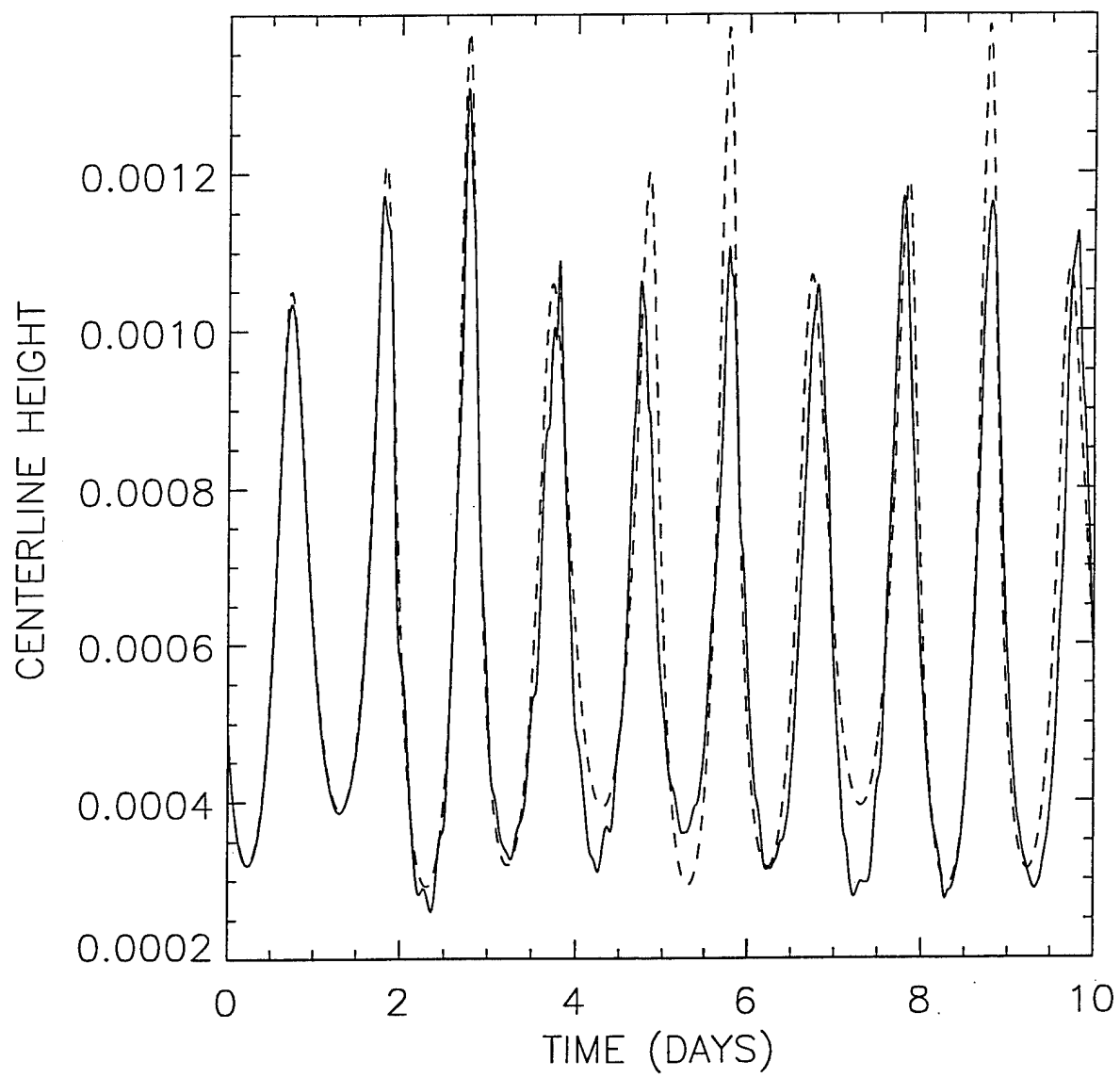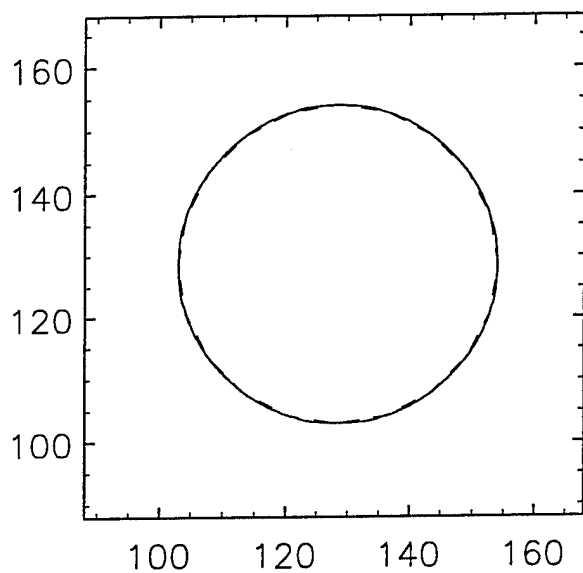
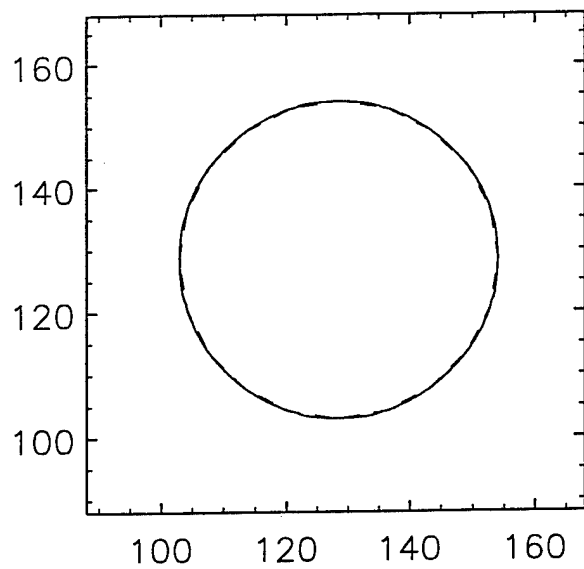INITIAL

DAY 0.1
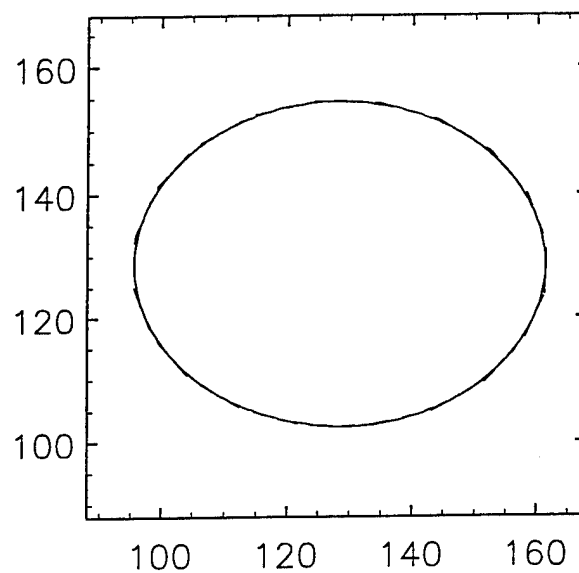
DAY 0.2
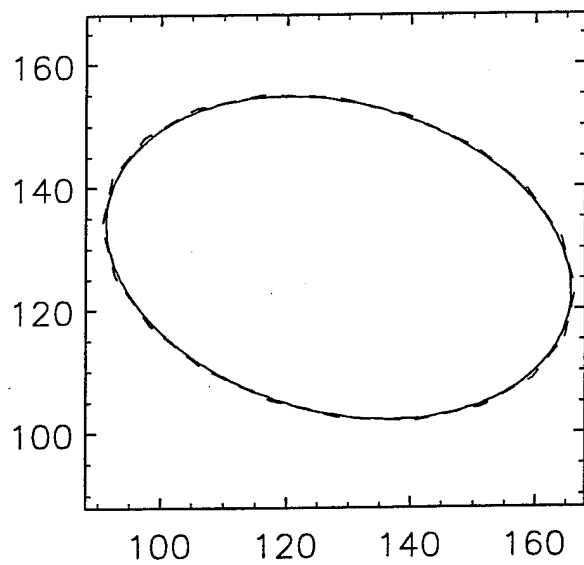
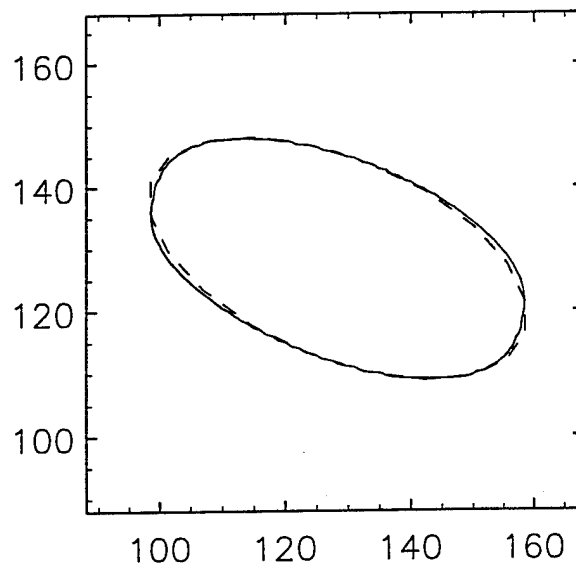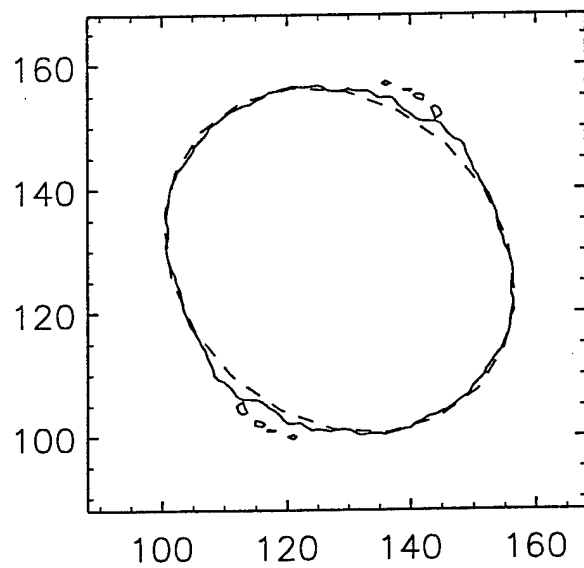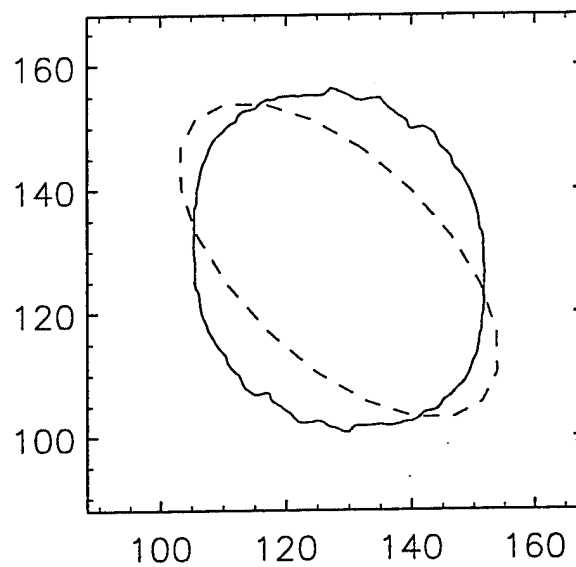DAY 0.3
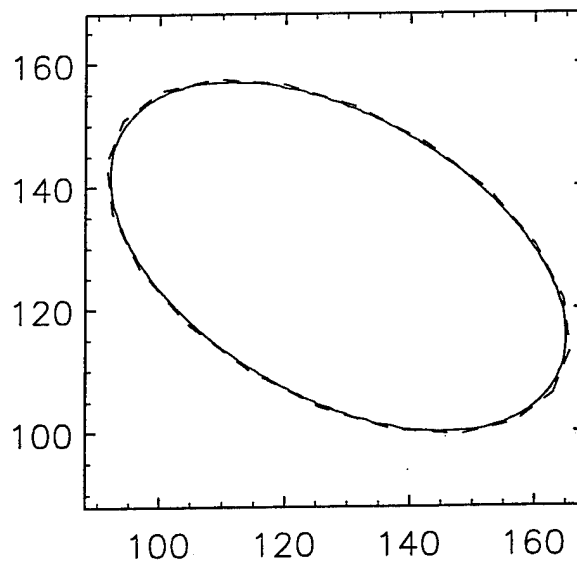
DAY 0.4
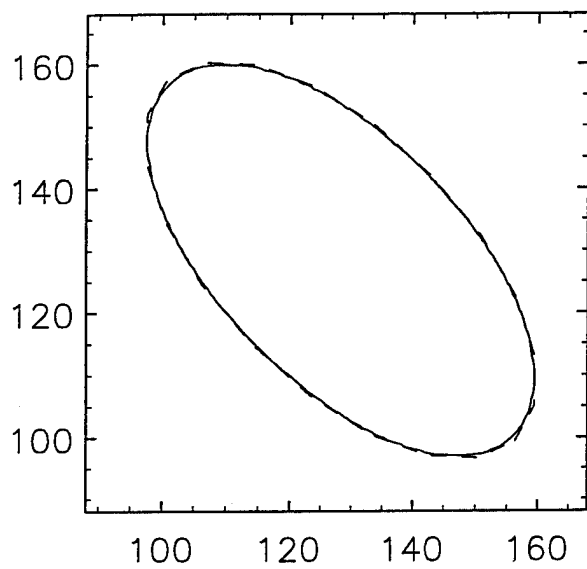
DAY 0.5
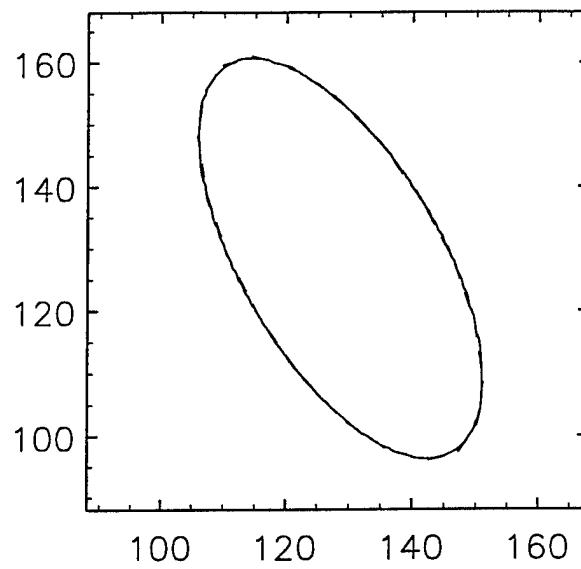
DAY 0.6
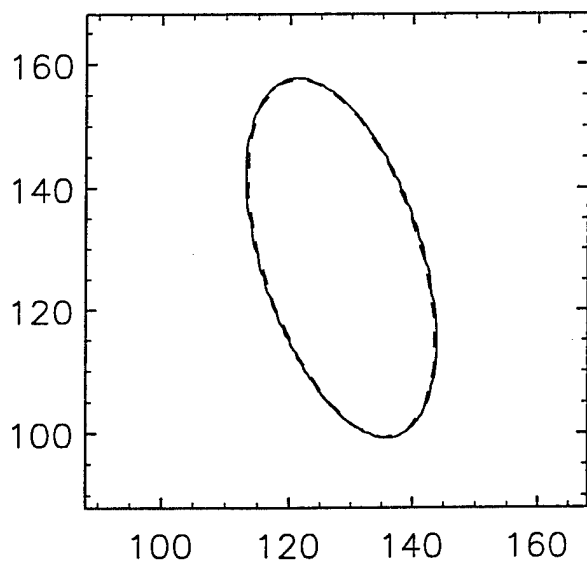
DAY 0.7
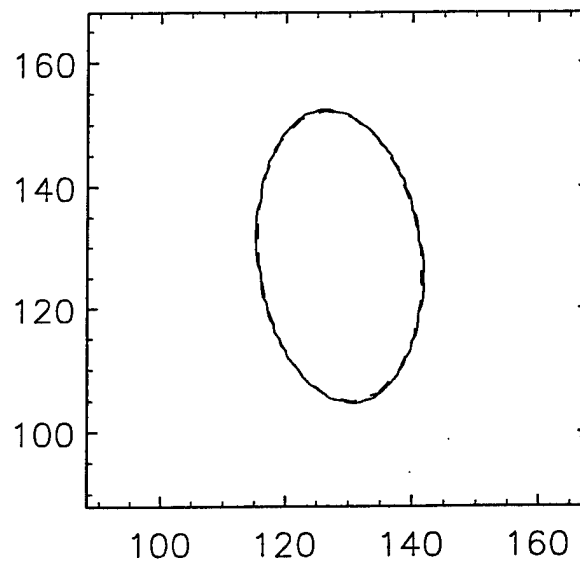
DAY 0.8
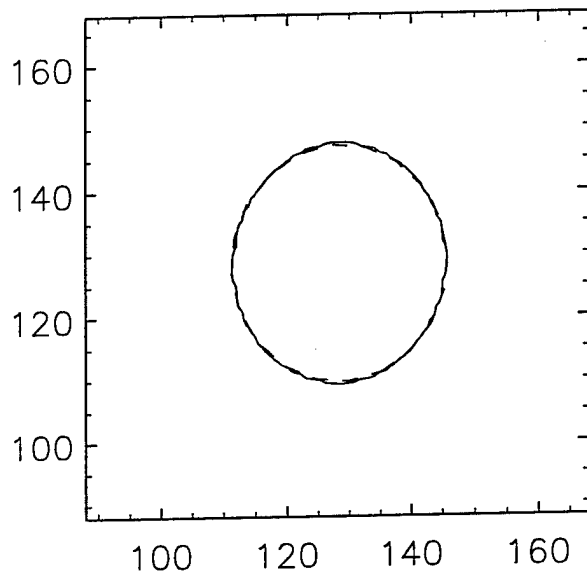
DAY 0.9

DAY 1.0
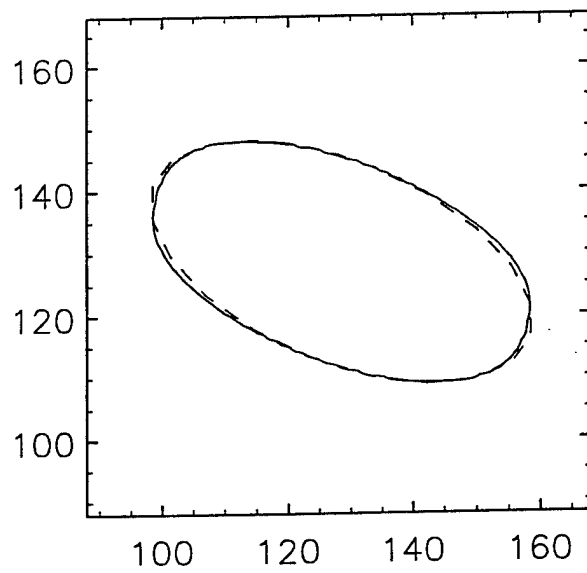
INITIAL

DAY 1.0

DAY 2.5

DAY 4.0
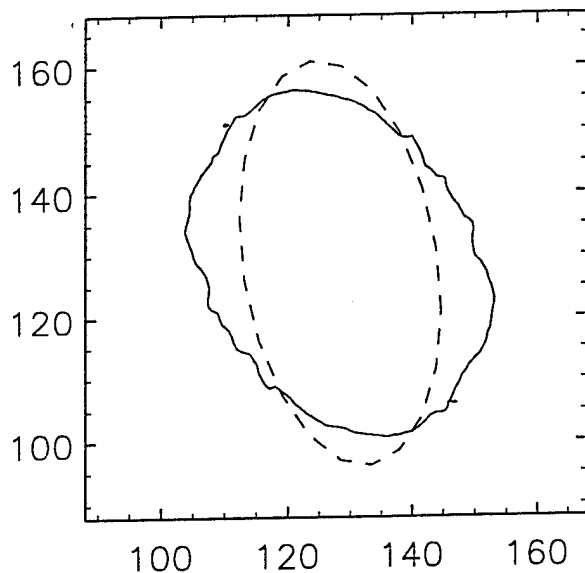
DAY 5.0

DAY 6.0

DAY 8.0

DAY 10.0

IN REPLY
REFER TO   DTIC-OCC

SUBJECT: Distribution Statements on Technical Documents

TO:
OFFICE OF NAVAL RESEARCH
CORPORATE PROGRAMS DIVISION
ONR 353
800 NORTH QUINCY STREET
ARLINGTON, VA 22217-5660

1. Reference: DoD Directive 5230.24, Distribution Statements on Technical Documents, 18 Mar 87.
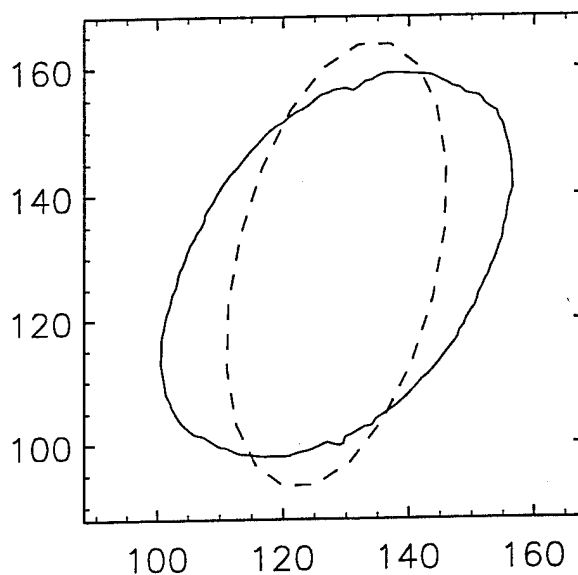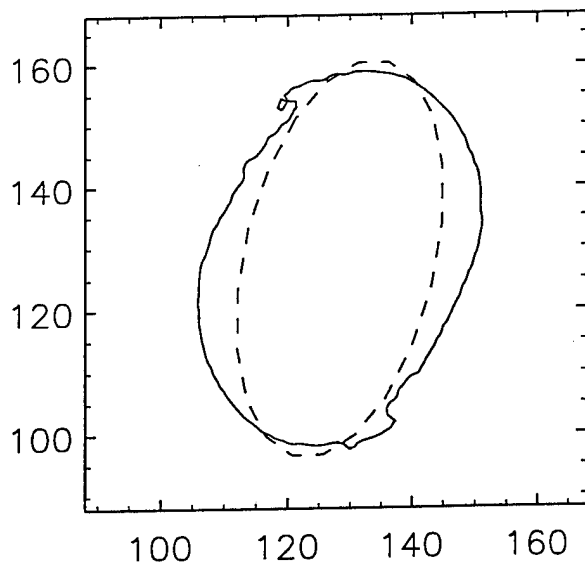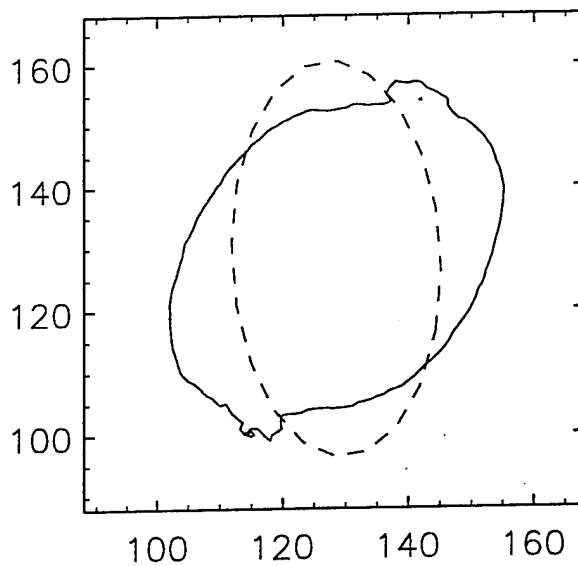
2. The Defense Technical Information Center received the enclosed report (referenced below) which is not marked in accordance with the above reference.

FINAL REPORT
N00014-93-1-0567
TITLE: A PARTICLE-IN-CELL MODEL
FOR GEOPHYSICAL FLUID FLOWS

3. We request the appropriate distribution statement be assigned and the report returned to DTIC within 5 working days.

4. Approved distribution statements are listed on the reverse of this letter. If you have any questions regarding these statements, call DTIC's Cataloging Branch, (703) 274-6837.

FOR THE ADMINISTRATOR:

1 Encl

GOPALAKRISHNAN NAIR
Chief, Cataloging Branch

FL-171
Jul 93

DISTRIBUTION STATEMENT A:

APPROVED FOR PUBLIC RELEASE: DISTRIBUTION IS UNLIMITED

DISTRIBUTION STATEMENT B:

DISTRIBUTION AUTHORIZED TO U.S. GOVERNMENT AGENCIES ONLY;
(Indicate Reason and Date Below). OTHER REQUESTS FOR THIS DOCUMENT SHALL BE REFERRED
TO (Indicate Controlling DoD Office Below).

DISTRIBUTION STATEMENT C:

DISTRIBUTION AUTHORIZED TO U.S. GOVERNMENT AGENCIES AND THEIR CONTRACTORS;
(Indicate Reason and Date Below). OTHER REQUESTS FOR THIS DOCUMENT SHALL BE REFERRED
TO (Indicate Controlling DoD Office Below).

DISTRIBUTION STATEMENT D:

DISTRIBUTION AUTHORIZED TO DOD AND U.S. DOD CONTRACTORS ONLY; (Indicate Reason
and Date Below). OTHER REQUESTS SHALL BE REFERRED TO (Indicate Controlling DoD Office Below).

DISTRIBUTION STATEMENT E:

DISTRIBUTION AUTHORIZED TO DOD COMPONENTS ONLY; (Indicate Reason and Date Below).
OTHER REQUESTS SHALL BE REFERRED TO (Indicate Controlling DoD Office Below).

DISTRIBUTION STATEMENT F:

FURTHER DISSEMINATION ONLY AS DIRECTED BY (Indicate Controlling DoD Office and Date
Below) or HIGHER DOD AUTHORITY.

DISTRIBUTION STATEMENT X:

DISTRIBUTION AUTHORIZED TO U.S. GOVERNMENT AGENCIES AND PRIVATE INDIVIDUALS
OR ENTERPRISES ELIGIBLE TO OBTAIN EXPORT-CONTROLLED TECHNICAL DATA IN ACCORDANCE
WITH DOD DIRECTIVE 5230.25, WITHHOLDING OF UNCLASSIFIED TECHNICAL DATA FROM PUBLIC
DISCLOSURE, 6 Nov 1984 (Indicate date of determination). CONTROLLING DOD OFFICE IS (Indicate
Controlling DoD Office).

The cited documents has been reviewed by competent authority and the following distribution statement is
hereby authorized.

_____   OFFICE OF NAVAL RESEARCH   _____
(Statement)   CORPORATE PROGRAMS DIVISION   (Controlling DoD Office Name)
                                 ONR 353
                                 800 NORTH QUINCY STREET
                                 ARLINGTON, VA 22217-5660

_____   _____
(Reason)   (Controlling DoD Office Address,
                                 DEBRA T. HUGHES   City, State, Zip)
                                 DEPUTY DIRECTOR
                                 CORPORATE PROGRAMS OFFICE   19 SEP 1995
_____   _____   _____
(Signature & Typed Name)   (Assigning Office)   (Date Statement Assigned)